POLITECNICO DI TORINO
Repository ISTITUZIONALE

Experimental Test of Nonlocality Limits from Relativistic Independence

Original
Experimental Test of Nonlocality Limits from Relativistic Independence / Atzori, F., Virzì, S., Rebufello, E., Avella, A., Piacentini, F., Cusini, I., Haka, H., Villa, F., Gramegna, M., Cohen, E., Degiovanni, I.P., Genovese, M.. - In: PRX QUANTUM. - ISSN 2691-3399. - 5:4(2024), pp. 1-15. [10.1103/PRXQuantum.5.040351]

Availability:
This version is available at: 11583/2996190 since: 2025-01-04T03:49:20Z

Publisher:
American Physical Society - APS

Published
DOI:10.1103/PRXQuantum.5.040351

Terms of use:

This article is made available under terms and conditions as specified in the corresponding bibliographic description in the repository

Publisher copyright

(Article begins on next page)

25 November 2026

Experimental Test of Nonlocality Limits from Relativistic Independence

Francesco Atzori,[1,2] Salvatore Virzì,[1] Enrico Rebufello,[1] Alessio Avella,[1] Fabrizio Piacentini,[1,*] Iris Cusini,[3] Henri Haka,[3] Federica Villa,[3] Marco Gramegna,[1] Eliahu Cohen,[4] Ivo Pietro Degiovanni,[1,5] and Marco Genovese[1,5]

[1] *Istituto Nazionale di Ricerca Metrologica (INRIM), Strada delle Cacce 91, I-10135 Torino, Italy*

[2] *Politecnico di Torino, Corso Duca degli Abruzzi 24, I-10129 Torino, Italy*

[3] *Dipartimento di Elettronica, Informazione e Bioingegneria, Politecnico di Milano, Piazza Leonardo da Vinci 32, 20133 Milano, Italy*

[4] *Faculty of Engineering and the Institute of Nanotechnology and Advanced Materials, Bar Ilan University, Ramat Gan 52900, Israel*

[5] *Istituto Nazionale di Fisica Nucleare (INFN), sezione di Torino, via P. Giuria 1, 10125 Torino, Italy*

(Received 2 May 2024; revised 14 November 2024; accepted 4 December 2024; published 30 December 2024)

Quantum correlations, like entanglement, represent the characteristic trait of quantum mechanics and pose essential issues and challenges to the interpretation of this pillar of modern physics. Although quantum correlations are largely acknowledged as a major resource to achieve quantum advantage in many tasks of quantum technologies, their full quantitative description and the axiomatic basis underlying them are still under investigation. Previous works have suggested that the origin of nonlocal correlations is grounded in principles capturing (from outside the quantum formalism) the essence of quantum uncertainty. In particular, the recently introduced principle of relativistic independence has given rise to a new bound intertwining local and nonlocal correlations. Here, we test such a bound by realizing together sequential and joint weak measurements on entangled photon pairs, allowing us to simultaneously quantify both local and nonlocal correlations by measuring incompatible observables on the same quantum system without collapsing its state, a task typically forbidden in the traditional (projective) quantum measurement framework. Our results demonstrate the existence of a fundamental limit on the extent of quantum correlations, shedding light on the profound role of uncertainty in both enabling and balancing them.

DOI: 10.1103/PRXQuantum.5.040351

I. INTRODUCTION

Investigating the very principles behind the laws of nature is one of the most captivating and intricate fields of scientific research. In this sense, quantum mechanics (QM) has demonstrated extraordinary predictive power when modeling the behavior of microscopic particles, also providing tools for technological boosts in fields such as communication [1–6], computation [7–11], imaging [12–17], hypothesis testing [18–21], metrology [22–26], and sensing [27–34], but a large debate is still ongoing in the scientific community about its foundational aspects. Particularly relevant is the investigation of nonlocal traits of quantum correlations among spatially separated parties [35], a research field that originated in 1935 with the Einstein-Podolsky-Rosen (EPR) paradox [36]. In 1964, Bell demonstrated how locality constrains the correlations between measurements on a bipartite system [37], proving that QM can exceed such a bound and, therefore, proving that its predictions are incompatible with those of any (classical) local hidden variable theory (LHVT) [37,38].

Later on, Tsirelson made an important step toward a quantitative analysis of quantum mechanical correlations, demonstrating that they are nevertheless bounded [39]. Subsequently, many physicists have devoted large efforts toward the investigation of quantum correlations and the first principles determining their strength [40–46], also trying to rule out probabilistic models exhibiting stronger-than-quantum correlations without violating the no-signaling principle [47]. However, none of these attempts has managed to account for the whole set of one- and two-point correlators in the simplest bipartite two-outcome scenario.

Recently, Carmi and Cohen have proposed a new fundamental principle, called relativistic independence (RI)

*Contact author: f.piacentini@inrim.it

Published by the American Physical Society under the terms of the Creative Commons Attribution 4.0 International license. Further distribution of this work must maintain attribution to the author(s) and the published article's title, journal citation, and DOI.

[48], stating that generalized local uncertainty relations (most generally defined, even outside quantum mechanics) cannot be affected by spacelike separated parties. Similarly to the works in Refs. [42,46], this approach emphasizes the major role of uncertainty in nature [49]. In addition, it allows us to derive familiar as well as novel bounds on quantum correlations, without explicitly assuming the full mathematical structure of QM. Indeed, correlations arising in theories complying with RI must satisfy certain bounds displaying an interplay between the nonlocal correlations shared among the parties of a multipartite system and the local correlations within the laboratory of each party (e.g., those related to quantum uncertainty) [48–50], ruling out theories admitting stronger-than-quantum correlations. Such RI-derived bounds generalize other known bounds on nonlocal quantum correlations and their experimental study is the main topic of this work.

The need to estimate both local and nonlocal correlations at once makes the experimental test of these bounds quite a challenging task, requiring us to quantify correlations among several incompatible (noncommuting) observables measured on the same quantum system without radically changing its state, which is prohibited by Heisenberg's uncertainty principle and by wave-function collapse in the standard projective-measurement scheme. In the following, we show how we have managed to test the RI bound by producing polarization-entangled photon pairs and performing a sequence of two weak measurements (WMs) [51–64] on both photons of each pair, allowing us to quantify all the correlations needed for testing the RI bound. Our results lead to a new experimental characterization of the set of nonlocal correlations within entangled states while emphasizing the role of local correlations in determining and bounding them. We also demonstrate the operative meaning of the bound stemming from RI, thereby clarifying its physical interpretation.

II. THEORETICAL FRAMEWORK

The correlations arising in quantum theory are much more intricate and interesting than those appearing in classical physics. In particular, because of quantum entanglement, measurements made on distant systems can lead to nonlocal correlations, i.e., correlations that are classically inexplicable because of their incompatibility with local realism (provided that the "free-choice assumption" or "statistical independence" holds [65–67]). This statement is captured by the violation of Bell inequalities [35,38], one of which is the Clauser-Horne-Shimony-Holt (CHSH) inequality:

$$|\mathcal{B}| \equiv |\langle A_1 B_1\rangle + \langle A_1 B_2\rangle + \langle A_2 B_1\rangle - \langle A_2 B_2\rangle| \leq 2, \quad (1)$$

where $\mathcal{B}$ is the so-called Bell-CHSH parameter and A_i and B_j are local dichotomic variables measured in the laboratories of two observers, Alice (A) and Bob (B), with two different measurement settings, i.e., $i,j = 1,2$. In quantum mechanics, they are represented by Hermitian operators, the nonlocal correlations of which may exceed the value of 2, reaching the aforementioned Tsirelson bound, i.e.,

$$|\mathcal{B}| \leq 2\sqrt{2}, \quad (2)$$

which determines the maximal extent of nonlocal quantum correlations. This inequality sets a bound on quantum correlations in bipartite scenarios without specifying how it is approached, i.e., what the bound on nonmaximal quantum correlations looks like and what makes them nonmaximal. Subsequently, richer bounds have been proposed [68–76] and tested [77].

In this work, we seek to advance the frontiers of this expedition toward the ultimate set of quantum correlations, exploring novel and more elaborate bounds on nonlocal (quantum) correlations. Remarkably, we experimentally show that these bounds on nonlocal correlations between Alice and Bob, as captured by $\mathcal{B}$, stem from the local correlations between their operators A_1 and A_2 on one side and B_1 and B_2 on the other. Moreover, they prove that a necessary condition for quantum correlations to achieve their maximum value is zero correlation between the two measurements on each party's laboratory.

A. Generalized uncertainty relations and the relativistic independence bound

The RI principle [48] stems from an attempt to quantify the strength of quantum correlations from outside the quantum formalism. It therefore aims at encoding two basic requirements, uncertainty and locality (in the sense that local uncertainty relations do not depend on measurement choices made by other parties), using a general statistical structure, namely, the covariance matrix, into which only the measured outcomes can be inserted (rather than other theoretical constructs such as Hermitian operators, commutators, etc.). The first point to be recalled here is the affinity between the Robertson-Schrödinger uncertainty relations and the positive semidefiniteness of the corresponding covariance matrix [49,50]—this will be illustrated in Eq. (4) below. The second point, which may require some conceptual leap, is the ability to transcend single-system uncertainty relations to bipartite (or, in general, multipartite) uncertainty relations. Finally, the RI principle ensures that such multipartite uncertainty relations encoded within covariance matrices will depend only on local parameters and, from that, it enables us to derive various bounds on quantum correlations. So, let our two observers, Alice and Bob, share a bipartite system. As stated above, they can measure the physical variables A_i and B_j and they can estimate the variances $\Delta^2_{A_i}$ and $\Delta^2_{B_j}$ and the covariances $C(B_j, A_i) = E_{B_j A_i} - E_{B_j} E_{A_i}$, where E_{A_j} and E_{B_j} are the one-point correlators for Alice

and Bob (respectively) and $E_{B_jA_i}$ are the two-point correlators between the two observers. The full system is governed by a generalized uncertainty relation that can be written as the following positive-semidefiniteness condition [48] (see Appendix A):

$$\mathbf{\Lambda}_{AB} = \begin{bmatrix} \mathbf{\Lambda}_B & \mathbf{C}(B,A) \\ \mathbf{C}^\dagger(B,A) & \mathbf{\Lambda}_A \end{bmatrix} \geq 0, \tag{3}$$

where $\mathbf{C}(B,A)$ is the cross-covariance matrix [78] between Alice and Bob, constituted by the $C(B_j,A_i)$ elements and representing the nonlocal correlations of the bipartite system, while $\mathbf{\Lambda}_A$ and $\mathbf{\Lambda}_B$ are the local covariance matrices for A and B, respectively, representing the local uncertainty relations of each subsystem, i.e., the familiar ones pertaining to A_1 and A_2 in Alice's laboratory and B_1 and B_2 in Bob's laboratory. Now, let Bob measure just one variable B_j, choosing one of the two available measurement settings. The generalized uncertainty relations are obtained by imposing positive semidefiniteness to a submatrix of $\mathbf{\Lambda}_{AB}$, i.e., the existence of some r_j from which stems the expression

$$\mathbf{\Lambda}^j_{AB} = \begin{bmatrix} \Delta^2_{B_j} & C(B_j,A_1) & C(B_j,A_2) \\ C^*(B_j,A_1) & \Delta^2_{A_1} & r_j \\ C^*(B_j,A_2) & r_j^* & \Delta^2_{A_2} \end{bmatrix} \geq 0. \tag{4}$$

LHVTs, QM, and even some models allowing for stronger-than-quantum correlations all satisfy Eq. (4). The r_j term is typically unmeasurable, as it corresponds to the nonobservable correlations between local variables and its form depends on the theory considered; e.g., in QM, one has $r_1 = r_2 \equiv r^Q = (\langle \hat{A}_1\hat{A}_2 + \hat{A}_2\hat{A}_1\rangle)/2 - \langle \hat{A}_1\rangle\langle \hat{A}_2\rangle$. In this case, Eq. (4) leads to the Schrödinger-Robertson uncertainty relation applied to the nonlocal operators B_jA_1 and B_jA_2 [48]. Unfortunately, the uncertainty principle and wave-function collapse do not allow us to measure r^Q together with all other quantities appearing in Eq. (4), at least within the traditional (projective) quantum measurement framework.

The fact that the r coefficient might depend on j means that, in principle, even in a spacelike separated scenario, Bob might still have a (nonlocal) influence on the generalized uncertainty relations. The RI principle forbids such nonlocal influence, stating that, in case of spacelike separation, the generalized uncertainty relations on Alice's (Bob's) side are independent of what occurs in Bob's (Alice's) laboratory, i.e.,

$$\mathbf{\Lambda}^j_A = \begin{bmatrix} \Delta^2_{A_1} & r_j \\ r_j^* & \Delta^2_{A_2} \end{bmatrix} \xrightarrow{\text{RI}} \mathbf{\Lambda}_A = \begin{bmatrix} \Delta^2_{A_1} & r \\ r^* & \Delta^2_{A_2} \end{bmatrix}. \tag{5}$$

From this formulation, one can derive the following bound (see Appendix A), displaying the interplay between local correlations within each party's laboratory and the nonlocal correlations arising between the two parties:

$$0 \leq \mathcal{RI} = \left|\frac{\mathcal{B}}{2\sqrt{2}}\right|^2 + \left(\text{Re}\left[\frac{r}{2\Delta_{A_2}\Delta_{A_1}}\right]\right)^2 \leq 1. \tag{6}$$

In the QM case, i.e., for $r = r^Q$, Eq. (6) becomes

$$0 \leq \mathcal{RI} = \left|\frac{\mathcal{B}}{2\sqrt{2}}\right|^2 + \Delta^2 \leq 1, \tag{7}$$

where $\mathcal{B}$ represents the nonlocal-correlations contribution and $\Delta = r^Q/2\Delta_{A_2}\Delta_{A_1}$, being proportional to the real part of the Pearson correlation coefficient $(\langle A_2A_1\rangle - \langle A_2\rangle\langle A_1\rangle)/\Delta_{A_2}\Delta_{A_1}$ [79] between the two measurements occurring in Alice's laboratory, accounts for the (local) correlations stemming from the uncertainty relations on Alice's side.

Equations (6) and (7) suggest that in quantum mechanics, but also more generally, large nonlocal correlations and large local correlations cannot coexist. Put differently, to have violations of the CHSH inequality, we must have small correlation between Alice's local choices (and similarly for Bob).

III. THE EXPERIMENT

To test the RI bound in Eq. (7), it is required to simultaneously evaluate the (nonlocal) correlations between A and B measurements and the (local) correlations between the two measurements performed either in laboratory A or laboratory B. This corresponds to evaluating, at once, the Bell-CHSH parameter $\mathcal{B}$ as well as the Pearson correlator between the two measurements realized in one of the laboratories, which we choose to be Alice's. In general, these measurements involve incompatible (noncommuting) observables, resulting in this task being forbidden by wave-function collapse and by Heisenberg's uncertainty principle in the traditional quantum measurement framework based on projective measurements. However, such a condition can be relaxed by implementing a sequence of two WMs per branch, as shown in Fig. 1, thus avoiding wave-function collapse (together with the inevitable entanglement breaking) at the cost of some tiny decoherence affecting the entangled state after the measurement process (for details, see Appendixes B and C). In this way, each entangled pair undergoes all the measurements (i.e., two per photon) needed to evaluate the local and nonlocal correlations forming the RI bound.

Specifically, our entangled-pair source (EPS) generates polarization-entangled photon pairs in the singlet state $|\psi_-\rangle = \frac{1}{\sqrt{2}}(|H_AV_B\rangle - |V_AH_B\rangle)$ (where H and V indicate, respectively, the horizontal and vertical polarization components) via degenerate spontaneous parametric down-conversion (SPDC) in a Sagnac interferometer.

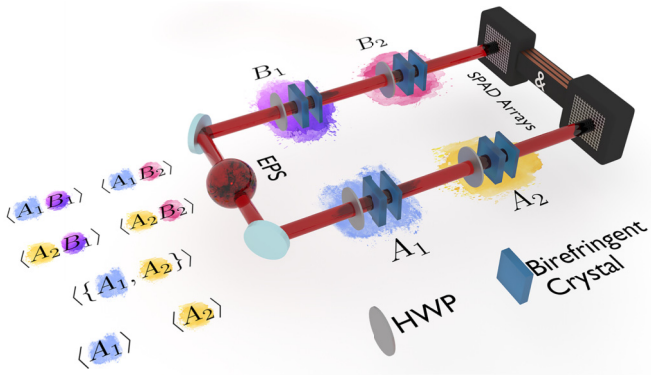


FIG. 1. The scheme of the experimental setup. Our entangled-pair source (EPS), based on spontaneous parametric down-conversion (SPDC) occurring in a Sagnac interferometer, generates entangled photon pairs in the state $|\psi_-\rangle = (|H_A V_B\rangle - |V_A H_B\rangle)/\sqrt{2}$, sending one photon to Alice (A) and the other to Bob (B). Both A and B implement two WMs in a row, each carried by a pair of birefringent crystals preceded by a half-wave plate (HWP), setting the measurement bases $i,j = 1,2$. In this way, our two-photon state undergoes joint [54–57,80] and sequential [58–61,63] WMs at once, preventing the $|\psi_-\rangle$ state wave function from collapsing, although at the cost of some small decoherence, allowing us to estimate all the measurement correlations (highlighted by different colors, with $\{A_1, A_2\} = (A_1A_2 + A_2A_1)$ required for testing the RI bound in Eq. (7). Finally, both photons A and B are detected by a two-dimensional (2D) spatially resolving detector with internal time-tagging capability, with dedicated coincidence electronics (labelled as "&"). A detailed description of the experimental setup is reported in Appendix B.

Both photons of each pair are spectrally filtered by narrow-band interference filters and then spatially filtered by coupling them into single-mode optical fibers, getting decoupled and collimated into Gaussian spatial distributions before being addressed to Alice and Bob (see Appendix B). This results in an overall initial wave function of our two-photon state of the form $|\Psi_{in}\rangle = |\psi_-\rangle \otimes |f_{x_A}\rangle \otimes |f_{y_A}\rangle \otimes |f_{x_B}\rangle \otimes |f_{y_B}\rangle$, where $\langle \zeta | f_\zeta \rangle = (1/(2\pi\sigma^2)^{1/4}) \exp\left(-(\zeta^2/4\sigma^2)\right)$ is the σ-wide Gaussian distribution of the photons in each transverse direction $\zeta = x_A, y_A, x_B, y_B$. The generated singlet state presents visibility $V^{in} = (N(+,-) + N(-,+) - N(+,+) - N(-,-))/(N(+,-) + N(-,+) + N(+,+) + N(-,-)) = 0.983 \pm 0.001$, where $N(\pm,\pm)$ is the number of two-photon counts registered while projecting photons A and B onto the states defining the diagonal-antidiagonal polarization basis, i.e., $|\pm\rangle = \frac{1}{\sqrt{2}}(|H\rangle \pm |V\rangle)$.

In both Alice's and Bob's laboratories, each WM is realized by exploiting the weak coupling between polarization and transverse momentum induced on the photon by a pair of thin birefringent crystals. The first crystal of the pair is the principal one and it induces a spatial walk-off (for the polarization component lying in the same plane as the crystal extraordinary (e) optical axis) in one of the two independent transverse directions x (for the first WM) and y (for the second one), leaving the two WMs occurring on each photon independent of each other. Anyway, this crystal also introduces a temporal delay and a phase shift between the H and V polarization components; the following "compensation" crystal, with the optical e axis oriented along the y axis (for the first WM) and the x axis (for the second one), is rotated along its optical e axis to compensate the temporal delay and nullify the phase shift without introducing any spatial decoherence. Each crystal pair is preceded by a half-wave plate (HWP), allowing us to select the polarization basis of the subsequent WM; the combined effect of HWP and crystal pair realizes the unitary transformation

$$\hat{U}_{\zeta_{jK}} = \exp\left(-\frac{i}{\hbar} g_{\zeta_{jK}} \hat{\Pi}(\vartheta_{K_j}) \otimes \hat{P}_{\zeta_{jK}}\right), \tag{8}$$

where $g_{\zeta_{jK}}$ is the coupling constant ($K = A, B$, $j = 1,2$, $\zeta_1 = x$, $\zeta_2 = y$) indicating the measurement strength, $\hat{\Pi}(\vartheta_{K_j})$ is the polarization projector along the direction described by the angle ϑ_{K_j}, and $\hat{P}_{\zeta_{jK}}$ is the transverse momentum of the photon on the optical plane of the crystal. For the WM condition to hold, the coupling constants $g_{\zeta_{jK}}$ must be much smaller than the spread of the pointer observable [51], i.e., in the specific case, of the width σ of the spatial Gaussian distribution of the photons (a thorough study of the effect of the measurement strength g on the WM can be found in Ref. [62]). This is needed to grant an (almost) negligible backaction of the measurement on the quantum system undergoing it, thus preventing wave-function collapse. Although, in principle, this would imply $(g_{\zeta_{jK}}/\sigma) \ll 1$, it has been shown [62] that for the kind of measurements needed in our experiment, it is already possible to achieve such a regime for $(g_{\zeta_{jK}}/\sigma) \lesssim 0.2$, as implemented in our setup (for details, see Appendix C).

After the four WMs, the entangled photon pairs are addressed to two spatially resolving detectors, allowing us to extract, for each twofold coincidence, the coordinates of the firing pixels and thus obtain the coincidence-count tensor $N(X_A, Y_A, X_B, Y_B)$, where X_A, Y_A and X_B, Y_B are the pixel coordinates in which the two photon of each pair impinge.

By relying just on WMs, i.e., without any postselection added after the weak couplings, we avoid wave-function collapse and manage to recover all the one- and two-point correlators needed for testing the RI bound. Indeed, considering only projections onto the real plane of the Bloch sphere, after the entangled pair undergoes the four WMs, one can extract the cross-correlations,

$$\begin{aligned}\langle \hat{\zeta}_{jA} \otimes \hat{\zeta}_{lB} \rangle_{\text{out}} &= \langle \Psi_{\text{out}} | \, \hat{\zeta}_{jA} \otimes \hat{\zeta}_{lB} \, | \Psi_{\text{out}} \rangle \\ &\simeq g_{\zeta_{jA}} g_{\zeta_{lB}} \langle \psi_- | \, \hat{\Pi}(\vartheta_{A_j}) \otimes \hat{\Pi}(\vartheta_{B_l}) \, | \psi_- \rangle \,,\end{aligned} \tag{9}$$

the single-branch sequential correlations,

$$\langle \hat{X}_K \hat{Y}_K \rangle_{\text{out}} = \langle \Psi_{\text{out}} | \hat{X}_K \hat{Y}_K | \Psi_{\text{out}} \rangle \simeq \frac{g_{x_K} g_{y_K}}{2} \langle \psi_- | \left\{ \hat{\Pi}(\vartheta_{K_1}), \hat{\Pi}(\vartheta_{K_2}) \right\} | \psi_- \rangle , \quad (10)$$

and the single-observable expectation values,

$$\langle \hat{\zeta}_{jK} \rangle_{\text{out}} = \langle \Psi_{\text{out}} | \hat{\zeta}_{jK} | \Psi_{\text{out}} \rangle \simeq g_{\zeta_{jK}} \langle \psi_- | \hat{\Pi}(\vartheta_{K_j}) | \psi_- \rangle , \quad (11)$$

where $j, l = 1, 2$ and $K = A, B$, the projectors $\hat{\Pi}(\vartheta_{K_j})$ are defined as $\hat{\Pi}(\vartheta_{K_j}) = (\hat{I} + \hat{\sigma}_z(\vartheta_{K_j})/2)$, the symbol $\{,\}$ indicates the anticommutator, and $|\Psi_{\text{out}}\rangle = \hat{U}_{y_A} \hat{U}_{x_A} \hat{U}_{y_B} \hat{U}_{x_B} |\Psi_{in}\rangle$ is the bipartite state after all weak couplings [for the sake of readability, we omit from Eq. (11) the tensor with the identity operator for the system subspace where no observable is evaluated]. Combining all these elements, one can evaluate the $\mathcal{RI}$ quantity in Eq. (7) as

$$\mathcal{RI} = \left| \frac{4 \left(\frac{\langle \hat{X}_A \hat{X}_B \rangle_{\text{out}}}{g_{X_A} g_{X_B}} - \frac{\langle \hat{X}_A \hat{Y}_B \rangle_{\text{out}}}{g_{X_A} g_{Y_B}} + \frac{\langle \hat{Y}_A \hat{X}_B \rangle_{\text{out}}}{g_{Y_A} g_{X_B}} + \frac{\langle \hat{Y}_A \hat{Y}_B \rangle_{\text{out}}}{g_{Y_A} g_{Y_B}} - \frac{\langle \hat{Y}_A \rangle_{\text{out}}}{g_{Y_A}} - \frac{\langle \hat{X}_B \rangle_{\text{out}}}{g_{X_B}} \right) + 2}{2\sqrt{2}} \right|^2 + \left| \frac{\frac{\langle \hat{X}_A \hat{Y}_A \rangle_{\text{out}}}{g_{X_A} g_{Y_A}} - \frac{\langle \hat{X}_A \rangle_{\text{out}} \langle \hat{Y}_A \rangle_{\text{out}}}{g_{X_A} g_{Y_A}}}{2 \sqrt{\left(\frac{\langle \hat{X}_A \rangle_{\text{out}}}{g_{X_A}} - \frac{\langle \hat{X}_A \rangle^2_{\text{out}}}{g^2_{\hat{X}_A}} \right) \left(\frac{\langle \hat{Y}_A \rangle_{\text{out}}}{g_{Y_A}} - \frac{\langle \hat{Y}_A \rangle^2_{\text{out}}}{g^2_{\hat{Y}_A}} \right)}} \right|^2 , \quad (12)$$

where the first term corresponds to the $|\mathcal{B}/2\sqrt{2}|^2$ value and the second one accounts for the Δ^2 component (a detailed description of the experimental setup can be found in Appendix B). By comparing Eqs. (9)–(12), one can appreciate how, in the weak-approximation regime (i.e., for a small coupling condition $g_{\zeta_{jK}}/\sigma \ll 1$, as in our case), the weakly measured $\mathcal{RI}$ is independent of the exact $g_{\zeta_{jK}}$ values, since they cancel out when substituting the expressions of Eqs. (9)–(11) in Eq. (12).

The experimental results are shown in Fig. 2. In the figure, we plot the results obtained for the RI bound in Eq. (7) by choosing on Alice's side the $\{0, \pi/2\}$ measurement basis (where $\{\gamma, \gamma + \pi/2\}$ is a basis defined by the rotation angle γ with respect to the $\{H, V\}$ basis) on the first measurement block and the $\{(\pi/4) + \delta, (3\pi/4) + \delta\}$ basis on the second one, while Bob performs the first and second measurements in his laboratory in the $\{\pi/8, 5\pi/8\}$ and $\{(3\pi/8) + \delta, (7\pi/8) + \delta\}$ bases, respectively. We choose these measurement bases because, for $\delta = 0$, they grant a maximal violation of the CHSH inequality, saturating the Tsirelson bound and maximizing the nonlocal correlations in our experiment (cancelling the local ones), as per Eq. (7). This means that in our setup, the parameter δ plays the role of an "angular mismatch" in the second measurement of each observer with respect to the one maximizing the Bell-CHSH parameter $|\mathcal{B}|$; by varying δ, we are able to quantitatively investigate the interplay between local and nonlocal correlations in our system.

In Fig. 2(a), we show the $\mathcal{RI}$ parameter, quantifying the total contributions due to the local correlations on Alice's laboratory and the nonlocal correlations between Alice's and Bob's measurements, as a function of δ. The experimental points (red dots) are in good agreement with the theoretical predictions (blue curve) within the experimental uncertainties (red vertical bars) and highlight how the nonlocal bound in Eq. (7) is always satisfied by the measurement correlations registered. On the other hand, in Fig. 2(b) we show the interplay between the two $\mathcal{RI}$ addenda, accounting, respectively, for nonlocal correlations of A and B (the reddish theoretical curve and the experimental dots) and the local correlations on Alice's side (the blue theoretical curve and the experimental dots). In particular, we observe how, for measurement choices closer to the ones allowing for a maximal violation of the CHSH inequality (i.e., for $\delta \in [-(\pi/4), \pi/4]$), there is a trade-off between local and nonlocal correlations, the latter reaching their maximum for $\delta = 0$, in correspondence with the RI bound saturation and in the complete absence of local correlations.

For this specific setting, our experiment yields $\mathcal{RI} = 0.98 \pm 0.11$, in excellent agreement with the theoretical predictions, just like all the other points reported in Fig. 2(a), which can be further confirmed by looking separately at the local and nonlocal terms of Eq. (7) shown in Fig. 2(b). Table I reports the different contributions to the experimental uncertainty obtained for $\mathcal{RI}(\delta = 0)$. Specifically, $\sigma_{\mathcal{RI},\text{stat}}$ is the statistical uncertainty given

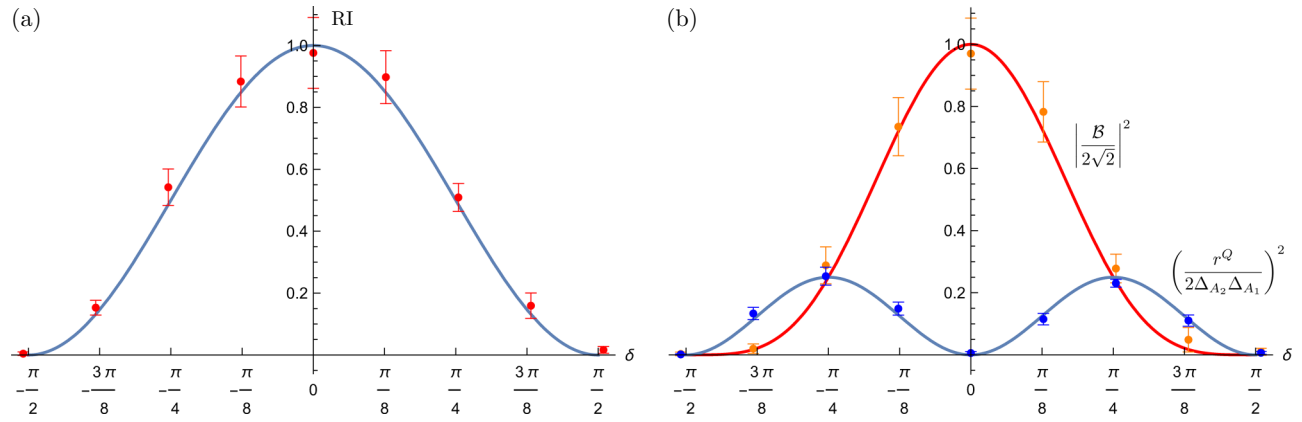


FIG. 2. The experimental test of the RI bound. (a) The overall RI: the test of the nonlocal-correlations bound in Eq. (7), derived from the RI principle, on the measurements performed by Alice and Bob on an entangled photon pair. Specifically, the $\mathcal{RI}$ parameter is evaluated with Alice measuring the polarization of photon A first in the $\{0, \pi/2\}$ basis and then in the $\{(\pi/4) + \delta, (3\pi/4) + \delta\}$ basis, with δ playing the role of a mismatch parameter with respect to the measurements, allowing for a maximal violation of the CHSH inequality, while Bob realizes subsequent polarization measurements on photon B in the $\{\pi/8, 5\pi/8\}$ and $\{(3\pi/8) + \delta, (7\pi/8) + \delta\}$ bases, respectively. (b) The separate contributions to RI: the interplay between local and nonlocal correlations within the bipartite system analyzed, highlighted by the behavior with respect to the mismatch parameter δ of the two contributions to $\mathcal{RI}$, i.e., the Tsirelson-bound-normalized Bell-CHSH parameter (red curve and orange dots), accounting for the nonlocal correlations; and the Pearson correlation coefficient between the two measurements A_1, A_2 (azure curve and blue dots), accounting for the local correlations in Alice's laboratory. In both plots, the dots and continuous curves represent the experimental results and the theoretical expectations, respectively. The uncertainty bars account for statistical uncertainties and all other uncertainty contributions (for details, see Appendix D). The plots show the (a) overall $\mathcal{RI}$ and (b) separate contributions to $\mathcal{RI}$.

by the data set collected during the experimental run, while $\sigma_{\mathcal{RI},\text{cal}}$ accounts for the uncertainties arising from the measurement-apparatus calibration procedure (for details on the experimental-uncertainties evaluation, see Appendix D).

IV. DISCUSSION AND CONCLUSIONS

The interplay between local and nonlocal correlations is of major relevance not just for the investigation of QM foundations [81] but also for quantum technologies, given the role of nonclassical correlations in quantum imaging and sensing, quantum metrology, quantum information processing, and computation. Our experiment allows the realization, for the first time, of simultaneous joint and sequential measurements on the same quantum system without collapsing its wave function, providing an elaborate characterization of the set of quantum correlations, as derived from the RI principle [48] and explicitly demonstrating an interplay between the amount of local and nonlocal correlations available in a quantum system. Moreover, our work substantiates the hypothesis [82,83] that quantum mechanics is as nonlocal as it is without violating causality, due to the existence of uncertainty. This result, following a rich and flourishing research path [84–94], represents a significant step toward understanding nonlocality in our most fundamental theory of nature [95].

On the practical side, such a measurement capability provides the key to investigating novel applications of quantum theory combining both local and nonlocal correlations. Prime among these are quantum computation and simulation, which employ entanglement and nonlocal correlations but balance them with local correlations to obtain optimal outcomes [96,97]. Furthermore, the proposed technique enables us to measure both local and nonlocal correlations on the same quantum system without inducing major decoherence on its state; this can, e.g., help in assessing the performance of near intermediate-scale quantum devices without significantly interfering with their operation.

TABLE I. The uncertainty budget for the average value of the quantity $\mathcal{RI}$ estimated in our experiment for $\delta = 0$, i.e., in correspondence with the RI bound saturation. The contributions to the overall experimental uncertainty $\sigma_{\mathcal{RI}}$ are (for details, see Appendix D) $\sigma_{\mathcal{RI},\text{stat}}$, the statistical-uncertainty contribution, and $\sigma_{\mathcal{RI},\text{cal}}$, the uncertainty contribution accounting for the setup calibration procedure.

δ	$\mathcal{RI}$	$\sigma_{\mathcal{RI}}$	$\sigma_{\mathcal{RI},\text{stat}}$	$\sigma_{\mathcal{RI},\text{cal}}$
0	0.98	0.11	0.08	0.08

ACKNOWLEDGMENTS

This work was financially supported by the projects QuaFuPhy (call "Trapezio" of the Fondazione San Paolo) and AQuTE [Ministry of University and Research (MUR), call "PRIN 2022," Grant No. 2022RATBS4], by the Israel

Science Foundation (Grant No. 2208/24), by the Israel Innovation Authority under Grants No. 70002 and No. 73795, by the Pazy Foundation, by the Israeli Ministry of Science and Technology, and by the Quantum Science and Technology Program of the Israeli Council of Higher Education. This work was also funded by the European Metrology Programme for Innovation and Research (EMPIR) project "Metrology for Testing the Implementation Security of Quantum Key Distribution Hardware" (MeTISQ) (Grant No. 19NRM06). This project received funding by the EMPIR program, cofinanced by the Participating States, and from the European Union (EU) Horizon 2020 Research and Innovation Programme. The results presented in this paper have also been achieved in the context of the following projects: QUantum Italy Deployment (QUID) and European QUantum ecOsystems (EQUO), which are funded by the European Commission in the Digital Europe Programme under Grant Agreements No. 101091408 and No. 101091561, and QU-TEST, which has received funding from the EU's Horizon Europe under Grant Agreement No. 101113901. We thank Yakir Aharonov, Avishy Carmi, and Avshalom Elitzur for enlightening discussions.

APPENDIX A: DERIVATION OF THE RELATIVISTIC INDEPENDENCE BOUND

As one can deduce from Eq. (4), Bob can nonlocally tamper with the generalized uncertainty relation encoded in that positive semidefinite matrix since, in general, r_j depends on Bob's choice j. The RI principle is the requirement for the generalized uncertainty relations to exist and remain independent of Bob's (Alice's) measurement choices, i.e., $r_j \equiv r$ [see Eq. (5)]. It has been shown [48] that the RI principle establishes a bound on local and shared correlations between Alice's and Bob's measurements. By the Schur complement [98] condition for positive semidefiniteness, one can write Eq. (4) as

$$\begin{aligned} M^{-1}\mathbf{\Lambda}_A M^{-1} &= \begin{bmatrix} 1 & \dfrac{r}{\Delta_{A_2}\Delta_{A_1}} \\ \dfrac{r^*}{\Delta_{A_2}\Delta_{A_1}} & 1 \end{bmatrix} \\ &\geq \begin{bmatrix} |\rho_{j2}|^2 & \rho_{j1}\rho_{j2} \\ \rho_{j1}^*\rho_{j2}^* & |\rho_{j1}|^2 \end{bmatrix}, \\ \begin{bmatrix} |\rho_{j2}|^2 & \rho_{j1}\rho_{j2} \\ \rho_{j1}^*\rho_{j2}^* & |\rho_{j1}|^2 \end{bmatrix} &= \Delta_{B_j}^{-2} M^{-1} \begin{bmatrix} C^*(B_j,A_2) \\ C^*(B_j,A_1) \end{bmatrix} \\ &\quad \times \begin{bmatrix} C(B_j,A_2) & C(B_j,A_1) \end{bmatrix} M^{-1}, \end{aligned} \tag{A1}$$

where M is a diagonal matrix with nonvanishing terms (not changing the positivity—just needed for transforming covariance into correlation), Δ_{A_2} and Δ_{A_1} are the local variances, and $\rho_{ji} = (E_{B_j A_i} - E_{B_j}E_{A_i})/\Delta_{B_j}\Delta_{A_i}$ is the Pearson correlation coefficient between A_i and B_j. The positive-semidefiniteness condition for a generic $n \times n$ matrix Γ implies that, for any vector $u_j \in \mathbb{C}^n$, one has $u_j \Gamma u_j^\dagger \geq 0$ [49]. If we consider $n = 2$ and $u_j = [(-1)^j, 1]$, by applying this property to Eq. (A1), we obtain

$$u_j \left(\begin{bmatrix} 1 & \dfrac{r}{\Delta_{A_1}\Delta_{A_0}} \\ \dfrac{r^*}{\Delta_{A_1}\Delta_{A_0}} & 1 \end{bmatrix} - \begin{bmatrix} |\rho_{1j}|^2 & \rho_{0j}\rho_{1j} \\ \rho_{0j}^*\rho_{1j}^* & |\rho_{0j}|^2 \end{bmatrix} \right) u_j^\dagger \geq 0, \tag{A2}$$

implying

$$2\left(1 + (-1)^j \operatorname{Re}\left(\frac{r}{\Delta_{A_2}\Delta_{A_1}}\right)\right) \geq |\rho_{1j} + (-1)^j \rho_{2j}|^2. \tag{A3}$$

By taking the square root on both sides, summing over Bob's choices $j = 1, 2$, and using the triangle inequality $|s| + |t| \geq |s + t|$, Eq. (A3) implies that

$$|\mathcal{B}| \leq \sqrt{2} \sum_{j=1,2} \sqrt{1 + (-1)^j \left(\frac{r}{\Delta_{A_2}\Delta_{A_1}}\right)}, \tag{A4}$$

where $\mathcal{B} = \langle \hat{A}_1\hat{B}_1 \rangle + \langle \hat{A}_1\hat{B}_2 \rangle + \langle \hat{A}_2\hat{B}_1 \rangle - \langle \hat{A}_2\hat{B}_2 \rangle$ is the Bell-CHSH parameter. Now, since $\sqrt{1-a} \leq 1 - a/2$ for $a \in [0, 1]$, the RI bound follows (upon squaring and rearranging):

$$0 \leq \mathcal{RI} = \left|\frac{\mathcal{B}}{2\sqrt{2}}\right|^2 + \left(\operatorname{Re}\left[\frac{r}{2\Delta_{A_2}\Delta_{A_1}}\right]\right)^2 \leq 1, \tag{A5}$$

which for the QM case ($r = r^Q$) becomes

$$0 \leq \mathcal{RI} = \left|\frac{\mathcal{B}}{2\sqrt{2}}\right|^2 + \left(\frac{r^Q}{2\Delta_{A_2}\Delta_{A_1}}\right)^2 \leq 1. \tag{A6}$$

APPENDIX B: EXPERIMENTAL DETAILS

A detailed scheme of our experimental setup is presented in Fig. 3. The setup consists of two main parts, one dedicated to the generation of polarization-entangled photon pairs and the other focused on their (weak) measurement and detection. The polarization-entangled two-photon state is produced by means of type-II spontaneous parametric down-conversion (SPDC) occurring in a periodically poled potassium titanyl phosphate (PPKTP) crystal hosted in a Sagnac interferometer. The PPKTP crystal is pumped by a cw laser at 405 nm, producing degenerate SPDC photon pairs at 810 nm. The down-converted photons, exiting the Sagnac interferometer in the singlet state $|\psi_-\rangle = (|H_A V_B\rangle - |V_A H_B\rangle)/\sqrt{2}$, are then

spectrally filtered, coupled to single-mode fibers, and collimated into Gaussian spatial modes $|f_{x_{A(B)}}\rangle \otimes |f_{y_{A(B)}}\rangle$ (with $\langle\zeta|f_\zeta\rangle = (1/(2\pi\sigma^2)^{1/4})\exp\left(-(\zeta^2/4\sigma^2)\right)$, where $\zeta = x, y$ and σ are the Gaussian distribution widths in both the x and y directions). The combination of both quarter- and half-wave plates ($\mathrm{QWP}_{A(B)}$ and $\mathrm{HWP}_{A(B)}$, respectively) allows us to compensate for the polarization changes due to the propagation within the single-mode fibers. In this way, we are able to send photon pairs in the state $|\Psi_{in}\rangle = |\psi_-\rangle \otimes |f_{x_A}\rangle \otimes |f_{y_A}\rangle \otimes |f_{x_B}\rangle \otimes |f_{y_B}\rangle$ to the A and B branches with visibility $V^{in} = (N(+,-) + N(-,+) - N(+,+) - N(-,-))/(N(+,-) + N(-,+) + N(+,+) + N(-,-)) = 0.983 \pm 0.001$, where $N(\alpha,\beta)$ is the number of two-photon counts registered while projecting photons A and B onto the $|\alpha\rangle$ and $|\beta\rangle$ states, respectively, and $|\pm\rangle = \frac{1}{\sqrt{2}}(|H\rangle \pm |V\rangle)$.

The subsequent WMs are carried out by exploiting the weak coupling between polarization and transverse momentum induced on each photon by pairs of thin calcite ($CaCO_3$) birefringent crystals. Each pair is composed of a principal crystal ($\mathrm{PC}_{A(B)}j$) and a compensation crystal ($\mathrm{CC}_{A(B)}j$), where $j = 1, 2$ indicates the position of the crystal pair in the measurement sequence. The optical e axes of $\mathrm{PC}_{A(B)}1$ and $\mathrm{PC}_{A(B)}2$ are oriented along perpendicular planes, specifically the z-x and y-z planes (with a $\pi/4$ angle with respect to the photon propagation direction z), in order to induce a spatial walk-off (for the polarization component lying in the same plane as the crystal e axis) in the two independent transverse directions x and y, to avoid affecting each other. Moreover, the $\mathrm{PC}_{A(B)}j$ crystals also introduce a temporal delay and a phase shift between the H and V polarization components, which need to be compensated. The compensation crystals $\mathrm{CC}_{A(B)}1$ and $\mathrm{CC}_{A(B)}2$ are mounted onto a motorized rotating stage, with the optical e axis lying, respectively, in the y and x direction (i.e., orthogonal to both the z direction and the principal crystal optical e axis). By rotating the compensation crystal along its optical axis, it becomes possible to restore the temporal delay and correct the phase without introducing any additional spatial decoherence. Each crystal pair is preceded by a half-wave plate ($\mathrm{HWP}_{A(B)}1$ and $\mathrm{HWP}_{A(B)}2$), enabling the choice of different polarization bases for each weak measurement implemented and allowing us to realize the unitary transformation in Eq. (8). Finally, entangled photons are detected by a 24×24 single-photon avalanche-diode array (SPADA), i.e., a single-photon detector with 2D spatial resolution composed of an array of SPADs with internal time-tagging electronics [99] able to record the arrival time (with 2-ns resolution) and the position of each detected photon pair. Lenses L1 and L2 constitute an imaging system needed to match the photon spatial-distribution dimensions with those of the SPADA active area. The internal time tagger of the SPADA allows us to extract the twofold coincidences and the coordinates of the firing pixels, constituting the coincidence-count tensor $N(X_A, Y_A, X_B, Y_B)$, where X_A, Y_A and X_B, Y_B are the pixel coordinates in which the two photons of each pair are detected.

APPENDIX C: ANALYSIS OF THE STATE DECOHERENCE INDUCED BY THE WEAK INTERACTIONS

After the four (weak) von Neumann couplings occurring in our setup (Fig. 1), the output state reads

$$|\Psi_{\mathrm{out}}\rangle = \hat{U}_{y_B}\hat{U}_{y_A}\hat{U}_{x_B}\hat{U}_{x_A}|\Psi_{in}\rangle = \hat{U}_{y_B}\hat{U}_{y_A}\hat{U}_{x_B}\hat{U}_{x_A}|\psi_-\rangle \otimes |f_{x_A}\rangle \otimes |f_{y_A}\rangle \otimes |f_{x_B}\rangle \otimes |f_{y_B}\rangle, \tag{C1}$$

where the $\hat{U}_{\zeta_{jK}}$ values ($j = 1, 2$, $K = A, B$) are the evolution operators defined in Eq. (8), $|\psi_-\rangle$ is the polarization-entangled singlet state generated by our EPS, and the $|f_{\zeta_{jK}}\rangle$ values are the (Gaussian) spatial components of the entangled-pair wave function. This means that the overall density matrix of the (pure) output state can be written as $\rho_{\mathrm{out}} = |\Psi_{\mathrm{out}}\rangle\langle\Psi_{\mathrm{out}}|$. If we restrict ourselves to the polarization subspace, the partial trace over the spatial degrees of freedom leads to the polarization-state density matrix $\rho_{\mathrm{out}}^{(\psi)} = \mathrm{Tr}_{x_A,y_A,x_B,y_B}(\rho_{\mathrm{out}})$, which presents some slight decoherence (due to the loss of information on the spatial degrees of freedom caused by the trace operation) with respect to the initial state $\rho_{in} = |\Psi_{in}\rangle\langle\Psi_{in}|$ because of the occurring WMs. We quantify this decoherence by comparing the purities $\mathcal{P}(\rho_{in}^{(\psi)})$ and $\mathcal{P}(\rho_{\mathrm{out}}^{(\psi)})$ (where $\mathcal{P}(\rho) = \mathrm{Tr}(\rho^2)$ and $\rho_{in}^{(\psi)} = \mathrm{Tr}_{x_A,y_A,x_B,y_B}(\rho_{in})$) of the polarization-state density matrix before and after the WMs, both extracted via quantum tomographic reconstruction [100]. For the sake of simplicity, let us now assume that all the weak couplings in our setup have approximately the same strength, i.e., $g_{\zeta_{jK}} \simeq g$, and consequently let us introduce the parameter $\Omega = 1 - \exp\left(-(g^2/8\sigma^2)\right)$, which plays the role of some "decoherence parameter" [101,102] (as we will see in the following). Given our weak-interaction regime, in which $(g/\sigma) \ll 1$ implies $\Omega \to 0$, the output-state purity $\mathcal{P}(\rho_{\mathrm{out}}^{(\psi)})$ can be expanded around $\Omega = 0$ as follows:

$$\begin{aligned}\mathcal{P}(\rho_{\mathrm{out}}^{(\psi)}) \approx 1 - 4\Omega + \frac{1}{2}\Omega^2 \,(22 &+ \cos[4(\alpha_1 - \alpha_2)] \\ &+ \cos[4(\alpha_1 - \beta_1)] + \cos[4(\alpha_2 - \beta_1)] \\ &+ \cos[4(\alpha_1 - \beta_2)] + \cos[4(\alpha_2 - \beta_2)] \\ &+ \cos[4(\beta_1 - \beta_2)]) + O(\Omega^3).\end{aligned} \tag{C2}$$

Remarkably, for the small interaction strength of the WMs implemented in our experiment ($g/\sigma \lesssim 0.2$, corresponding to $\Omega \lesssim 0.005$, clear evidence of the weakness of

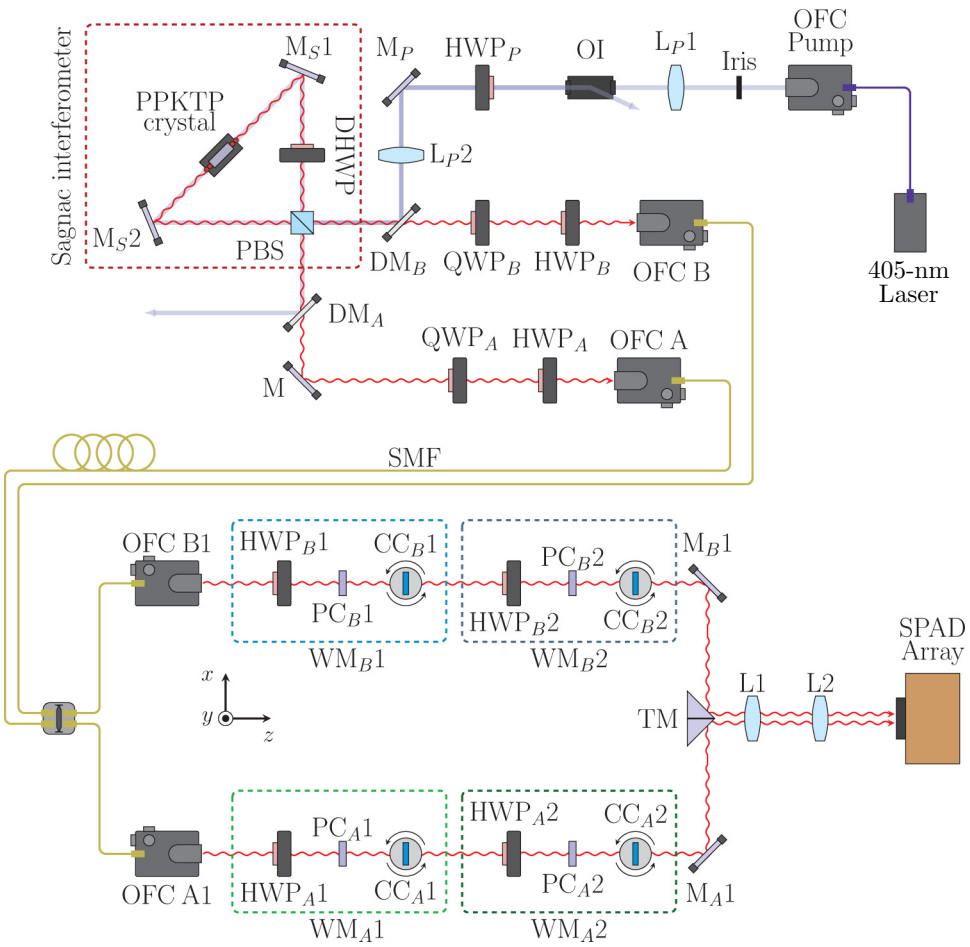


FIG. 3. A representation of our experimental setup. Polarization-entangled photon pairs in the singlet state $|\psi_-\rangle = (|H_A V_B\rangle - |V_A H_B\rangle)/\sqrt{2}$ are generated in a Sagnac interferometer, coupled to an optical fiber, and collimated in a Gaussian spatial mode. Then, each photon undergoes two weak measurements in a row, each realized by a pair of birefringent crystals preceded by a HWP. At the end of the measurement process, the photon pair is detected by a 24×24 SPAD array with 2D spatial resolution. CC, compensation crystal; DHWP, dual half-wave plate; DM, dichroic mirror; HWP, half-wave plate; Iris, pump beam pinhole; L1 and L2, imaging-system lenses; L_p1 and L_p2, pump-beam focusing lenses; M, mirror; OFC, optical-fiber coupler; OI, optical isolator; PBS, polarizing beam splitter; PC, principal crystal; PPKTP, periodically poled potassium titanyl phosphate; QWP, quarter-wave plate; SMF, single-mode fiber; SPAD, single-photon avalanche diode; TM, triangular mirror; WM, weak measurement.

our measurements), the angular dependence of Eq. (C2) becomes negligible and the amount of decoherence in $\rho_{\text{out}}^{(\psi)}$ is the same for every choice of α_i and β_j.

Since the singlet state produced by our EPS presents an initial purity of 0.98, the induced decoherence should lead to an output-state purity $\mathcal{P}(\rho_{\text{out}}^{(\psi)}) \simeq 0.96$. The tomographically reconstructed output state for $\delta = 0$, on the other hand, features $\mathcal{P}(\rho_{\text{out}}^{(\psi)}) = 0.94$, quite close to the theoretical expectations, with the further purity drop most likely due to the nonoptimality of our optical components (not included in the theoretical analysis). Nevertheless, these results demonstrate how, after the WM process, the polarization state has just suffered a slight decoherence, instead of the full wave-function collapse eventually induced by strong (projective) measurements.

APPENDIX D: STATISTICAL ANALYSIS

In our experiment, we perform six data acquisitions, with different setup configurations. To calibrate the system, we send only either horizontally (H) or vertically (V) polarized photons to both A and B, by generating the two-photon separable states $|H_A V_B\rangle$ and $|V_A H_B\rangle$. Considering that the first birefringent crystal pairs in A and B (composed, respectively, of the PC_K1 and CC_K1 crystals in Fig. 3, where $K = A, B$) shift the H-polarized photons along the x transverse direction, while the second crystal pairs (formed by the PC_K2 and CC_K2 crystals) shift the V-polarized photons along y, the $|H_A V_B\rangle$ and $|V_A H_B\rangle$ states allow us to obtain (via a linear regression of several subsets and subsequent average) the spatial distribution centers for the H and V photons. From these acquisitions, we can also

extract the photon-distribution centers in the unperturbed case and, as a consequence, the $g_{\zeta_{jK}}$ values.

For convenience, the center of the unperturbed (shifted) spatial distribution is dubbed $\tilde{\zeta}_{K,0(1)}$ ($\zeta = x, y$; $K = A, B$). In light of this, the WM interaction intensities can be obtained as (for further details on the connection between spatial distributions and the WM interaction intensity, see Ref. [103,104]):

$$g_{\zeta_K} = \tilde{\zeta}_{K,1} - \tilde{\zeta}_{K,0}. \tag{D1}$$

Then, we set HWP_P to produce the singlet state $|\psi_-\rangle$, and the HWPs on A (HWP_A1 and HWP_A2) and B (HWP_B1 and HWP_B2) sides so as to get a full data set allowing us to evaluate the $\mathcal{RI}$ bound for a fixed "mismatch parameter" δ, obtaining a set of ζ_K ($\zeta = x, y$; $K = A, B$) values. Finally, we remove the $\mathrm{PC}_K m$ and $\mathrm{CC}_K m$ birefringent crystals ($m = 1, 2$) and perform three data acquisitions with only HWPs in the photon paths. In the first acquisition, we keep the same $\mathrm{HWP}_K m$ angles as the $\mathcal{RI}$ acquisition and send the singlet state $|\psi_-\rangle$ as input. Conversely, the second and third acquisitions are performed with all the $\mathrm{HWP}_K m$ angles on their 0 values and with $|H_A V_B\rangle$ and $|V_A H_B\rangle$, respectively, as input states. This allows us to evaluate (and eventually compensate for) the unwanted spatial deviation induced on the photons by the HWP position change between the calibration and $\mathcal{RI}$ acquisitions, which we dub as $\tilde{\zeta}_{K,\mathrm{shift}}$. Once again, they are extracted by linear regression and subsequent averaging.

The left-hand side of the RI bound in Eq. (7) is the square sum of two terms, one ($\left|\mathcal{B}/2\sqrt{2}\right|$) concerning the nonlocal correlations between Alice and Bob and the other (Δ) accounting for the local correlations on Alice's side. Following the same mathematical derivation leading to Eq. (7), we can express the Bell-CHSH parameter $\mathcal{B}$ as (from now on, we drop the $_{\mathrm{out}}$ subscript for the sake of readability):

$$\mathcal{B} = 4\left(\frac{\left\langle \hat{X}_A \hat{X}_B \right\rangle}{g_{X_A} g_{X_B}} - \frac{\left\langle \hat{X}_A \hat{Y}_B \right\rangle}{g_{X_A} g_{Y_B}} + \frac{\left\langle \hat{Y}_A \hat{X}_B \right\rangle}{g_{Y_A} g_{X_B}} + \frac{\left\langle \hat{Y}_A \hat{Y}_B \right\rangle}{g_{Y_A} g_{Y_B}} - \frac{\left\langle \hat{Y}_A \right\rangle}{g_{Y_A}} - \frac{\left\langle \hat{X}_B \right\rangle}{g_{X_B}}\right) + 2. \tag{D2}$$

The expressions $\left\langle \hat{\zeta}_K \right\rangle$ ($\zeta = X, Y$; $K = A, B$) and $\left\langle \hat{\zeta}_A \otimes \hat{\zeta}_B \right\rangle$ ($\zeta = X, Y$; $K = A, B$) can be evaluated as

$$\left\langle \hat{\zeta}_K \right\rangle = \left\langle \zeta_K - \tilde{\zeta}_{K,0} - \tilde{\zeta}_{K,\mathrm{shift}} \right\rangle, \tag{D3}$$

$$\left\langle \hat{\zeta}_A \otimes \hat{\zeta}_B \right\rangle = \left\langle (\zeta_A - \tilde{\zeta}_{A,0} - \tilde{\zeta}_{A,\mathrm{shift}})(\zeta_B - \tilde{\zeta}_{B,0} - \tilde{\zeta}_{B,\mathrm{shift}}) \right\rangle. \tag{D4}$$

Substituting in Eq. (D2), we obtain the following expression for the Bell-CHSH parameter:

$$\begin{aligned}\mathcal{B} = 4\Bigg\langle & \frac{(X_A - \tilde{X}_{A,0} - \tilde{X}_{A,\mathrm{shift}})(X_B - \tilde{X}_{B,0} - \tilde{X}_{B,\mathrm{shift}})}{(\tilde{X}_{A,1} - \tilde{X}_{B,0})(\tilde{X}_{B,1} - \tilde{X}_{B,0})} \\ & - \frac{(X_A - \tilde{X}_{A,0} - \tilde{X}_{A,\mathrm{shift}})(Y_B - \tilde{Y}_{B,0} - \tilde{Y}_{B,\mathrm{shift}})}{(\tilde{X}_{A,1} - \tilde{X}_{A,0})(\tilde{Y}_{B,1} - \tilde{Y}_{B,0})} \\ & + \frac{(Y_A - \tilde{Y}_{A,0} - \tilde{Y}_{A,\mathrm{shift}})(X_B - \tilde{X}_{B,0} - \tilde{X}_{B,\mathrm{shift}})}{(\tilde{Y}_{A,1} - \tilde{y}_{A,0})(\tilde{X}_{B,1} - \tilde{X}_{B,0})} \\ & + \frac{(Y_A - \tilde{Y}_{A,0} - \tilde{Y}_{A,\mathrm{shift}})(Y_B - \tilde{Y}_{B,0} - \tilde{Y}_{B,\mathrm{shift}})}{(\tilde{Y}_{A,1} - \tilde{Y}_{A,0})(\tilde{Y}_{B,1} - \tilde{Y}_{B,0})} \\ & - \frac{Y_A - \tilde{Y}_{A,0} - \tilde{Y}_{A,\mathrm{shift}}}{\tilde{Y}_{A,1} - \tilde{Y}_{A,0}} - \frac{X_{1B} - \tilde{X}_{B,0} - \tilde{X}_{B,\mathrm{shift}}}{\tilde{X}_{B,1} - \tilde{X}_{B,0}}\Bigg\rangle + 2.\end{aligned} \tag{D5}$$

Conversely, the Δ quantity in Eq. (7) can be expressed as

$$\begin{aligned}\Delta &= \frac{\frac{\left\langle \hat{X}_A \hat{Y}_A \right\rangle}{g_{X_A} g_{Y_A}} - \frac{\left\langle \hat{X}_A \right\rangle \left\langle \hat{Y}_A \right\rangle}{g_{X_A} g_{Y_A}}}{2\sqrt{\left(\frac{\left\langle \hat{X}_A \right\rangle}{g_{X_A}} - \frac{\left\langle \hat{X}_A \right\rangle^2}{g_{X_A}^2}\right)\left(\frac{\left\langle \hat{Y}_A \right\rangle}{g_{Y_A}} - \frac{\left\langle \hat{Y}_A \right\rangle^2}{g_{Y_A}^2}\right)}} \\ &= \frac{\left\langle \hat{X}_A \hat{Y}_A \right\rangle - \left\langle \hat{X}_A \right\rangle \left\langle \hat{Y}_A \right\rangle}{2\sqrt{\left(g_{X_A}\left\langle \hat{X}_A \right\rangle - \left\langle \hat{X}_A \right\rangle^2\right)\left(g_{Y_A}\left\langle \hat{Y}_A \right\rangle - \left\langle \hat{Y}_A \right\rangle^2\right)}} \\ &= \frac{C_{xy,A}}{2\sqrt{S_{x,A} S_{y,A}}},\end{aligned} \tag{D6}$$

where

$$C_{xy,A} = \left\langle \hat{X}_A \hat{Y}_A \right\rangle - \left\langle \hat{X}_A \right\rangle \left\langle \hat{Y}_A \right\rangle, \tag{D7}$$

$$S_{\zeta,A} = g_{\zeta_A}\left\langle \hat{\zeta}_A \right\rangle - \left\langle \hat{\zeta}_A \right\rangle^2, \tag{D8}$$

with $\zeta = x, y$ and $\hat{\zeta} = \hat{X}, \hat{Y}$. Substituting $\hat{\zeta}_K = \zeta_K - \tilde{\zeta}_{K,0} - \tilde{\zeta}_{K,\mathrm{shift}}$ into Eq. (D7), one obtains

$$C_{xy,A} = \left\langle \left(X_A - \tilde{X}_{A,0} - \tilde{X}_{A,\mathrm{shift}}\right)\left(Y_A - \tilde{Y}_{A,0} - \tilde{Y}_{A,\mathrm{shift}}\right)\right\rangle$$

$$- \left\langle X_A - \tilde{X}_{A,0} - \tilde{X}_{A,\text{shift}} \right\rangle \left\langle Y_A - \tilde{X}_{A,0} - \tilde{Y}_{A,\text{shift}} \right\rangle$$
$$= \langle X_A Y_A \rangle - \langle X_A \rangle \langle Y_A \rangle , \tag{D9}$$

which follows from linearity of the expectation value. By comparing Eq. (D7) with Eq. (D9), it appears evident how $C_{xy,A}$ turns out to be independent of both the set of coordinates of the unperturbed distribution center $(\tilde{X}_{A,0}, \tilde{Y}_{A,0})$ and the one accounting for the unwanted deviations induced by the HWPs $(\tilde{X}_{A,\text{shift}}, \tilde{Y}_{A,\text{shift}})$.

Furthermore, simple manipulation shows that

$$S_{\zeta,A} = \left(\langle \zeta_A \rangle - \tilde{\zeta}_{A,0} - \tilde{\zeta}_{A,\text{shift}} \right) \left(\tilde{\zeta}_{A,1} + \tilde{\zeta}_{A,\text{shift}} - \langle \zeta_A \rangle \right), \tag{D10}$$

allowing us to write Δ as

$$\Delta = \frac{\langle X_A Y_A \rangle - \langle X_A \rangle \langle Y_A \rangle}{2\sqrt{\left(\langle X_A \rangle - \tilde{X}_{A,0} - \tilde{X}_{A,\text{shift}} \right) \left(\tilde{X}_{A,1} + \tilde{X}_{A,\text{shift}} - \langle X_A \rangle \right)}} \times \frac{1}{\sqrt{\left(\langle Y_A \rangle - \tilde{Y}_{A,0} - \tilde{Y}_{A,\text{shift}} \right) \left(\tilde{Y}_{A,1} + \tilde{Y}_{A,\text{shift}} - \langle Y_A \rangle \right)}}. \tag{D11}$$

For each quantity $\mathcal{P} = \{\mathcal{B}, \Delta, \mathcal{RI}\}$, the associated experimental uncertainty is evaluated as

$$\sigma_{\mathcal{P}} = \sqrt{\sigma^2_{\mathcal{P},\text{stat}} + \sigma^2_{\mathcal{P},\text{cal}}}, \tag{D12}$$

where $\sigma_{\mathcal{P},\text{stat}}$ represents the statistical contribution to the overall uncertainty and

$$\sigma_{\mathcal{P},\text{cal}} = \sqrt{\sum_{\substack{\tilde{\zeta}=\tilde{X},\tilde{Y} \\ K=A,B \\ j=0,1}} \left(\frac{\partial \mathcal{P}}{\partial \tilde{\zeta}_{K,j}} \right)^2 \sigma^2_{\mathcal{P},\tilde{\zeta}_{K,j}} + \sum_{\substack{\tilde{\zeta}=\tilde{X},\tilde{Y} \\ K=A,B}} \left(\frac{\partial \mathcal{P}}{\partial \tilde{\zeta}_{K,\text{shift}}} \right)^2 \sigma^2_{\mathcal{P},\tilde{\zeta}_{K,\text{shift}}}} \tag{D13}$$

is the uncertainty associated with the calibration procedure (including the HWP-induced spatial shift), with $\sigma_{\mathcal{P},\tilde{\zeta}_{K,j}}$ being the uncertainty contribution to $\sigma_{\mathcal{P},\text{cal}}$ depending on the calibration parameters $\tilde{\zeta}_{K,j}$ and $\sigma_{\mathcal{P},\tilde{\zeta}_{K,\text{shift}}}$ being the uncertainty contribution associated with the spatial shift induced by the HWPs.

To evaluate the statistical uncertainty $\sigma_{\mathcal{P},\text{stat}}$, we assume the following hypotheses:

(1) Let $\zeta_{K,i}$, i.e., the position ζ of the ith detected photon on the branch K, be a random variable with variance $V^2\left[\zeta_{K,i}\right] = V^2_{\zeta_K}$ (where $\zeta = X, Y$).
(2) For independent events, the covariance condition $\sigma_{X_{K,i}Y_{K',j}} = \sigma_{X_K Y_{K'}} \delta_{ij}$ is satisfied.

Then, we can write $\sigma_{\mathcal{P},\text{stat}}$ as

TABLE II. The uncertainty budget for the average value of the Bell-CHSH parameter $\mathcal{B}$ estimated in our experiment. $\sigma_{\mathcal{B}}$, Total uncertainty; $\sigma_{\mathcal{B},\text{stat}}$, statistical-uncertainty contribution; $\sigma_{\mathcal{B},\text{cal}}$, uncertainty contribution due to the setup calibration procedure and the correction of the HWP-related (unwanted) spatial shifts.

δ	$\mathcal{B}$	$\sigma_{\mathcal{B}}$	$\sigma_{\mathcal{B},\text{stat}}$	$\sigma_{\mathcal{B},\text{cal}}$
$-\pi/2$	-0.15	0.16	0.11	0.11
$-3\pi/8$	-0.40	0.15	0.11	0.11
$-\pi/4$	-1.52	0.16	0.12	0.10
$-\pi/8$	-2.42	0.15	0.11	0.10
0	-2.79	0.16	0.12	0.11
$\pi/8$	-2.50	0.16	0.11	0.11
$\pi/4$	-1.49	0.12	0.05	0.11
$3\pi/8$	-0.63	0.25	0.12	0.22
$\pi/2$	-0.28	0.16	0.12	0.11

TABLE III. The uncertainty budget for Alice's local correlations parameter Δ estimated in our experiment. σ_{Δ}, Total uncertainty; $\sigma_{\Delta,\text{stat}}$, statistical-uncertainty contribution; $\sigma_{\Delta,\text{cal}}$, uncertainty contribution due to the setup calibration procedure and the HWP-related (unwanted) spatial shifts.

δ	Δ	σ_{Δ}	$\sigma_{\Delta,\text{stat}}$	$\sigma_{\Delta,\text{cal}}$
$-\pi/2$	-0.037	0.027	0.027	6.6×10^{-5}
$-3\pi/8$	-0.365	0.027	0.027	5.6×10^{-4}
$-\pi/4$	-0.503	0.029	0.029	1.1×10^{-3}
$-\pi/8$	-0.386	0.027	0.027	5.0×10^{-4}
0	-0.076	0.031	0.031	1.7×10^{-3}
$\pi/8$	0.339	0.027	0.027	4.3×10^{-4}
$\pi/4$	0.480	0.013	0.013	9.2×10^{-4}
$3\pi/8$	0.333	0.027	0.027	6.4×10^{-4}
$\pi/2$	-0.081	0.030	0.030	1.7×10^{-4}

TABLE IV. The uncertainty budget for the experimental estimation of the three elements presented in Eq. (D15), i.e., the RI parameter $\mathcal{RI}$; $\mathcal{RI}_{\mathcal{B}} = |\mathcal{B}/2\sqrt{2}|^2$, accounting for the contribution of nonlocal correlations to $\mathcal{RI}$; $\mathcal{RI}_{\Delta} = \Delta^2$, constituting the $\mathcal{RI}$ part due to local correlations. $\sigma_{\mathcal{RI}}$, Overall uncertainty associated with $\mathcal{RI}$; $\sigma_{\mathcal{RI},\text{stat}}$, statistical-uncertainty contribution to $\sigma_{\mathcal{RI}}$; $\sigma_{\mathcal{RI},\text{cal}}$, uncertainty contribution to $\sigma_{\mathcal{RI}}$ due to the setup calibration procedure and the correction of the HWP-related (unwanted) spatial shifts; $\sigma_{\mathcal{RI}_{\mathcal{B}}}$, overall uncertainty associated with the $\mathcal{RI}$ nonlocal component $\mathcal{RI}_{\mathcal{B}}$; $\sigma_{\mathcal{RI}_{\Delta}}$, overall uncertainty associated with the $\mathcal{RI}$ local component $\mathcal{RI}_{\Delta}$.

δ	$\mathcal{RI}$	$\sigma_{\mathcal{RI}}$	$\sigma_{\mathcal{RI},\text{stat}}$	$\sigma_{\mathcal{RI},\text{cal}}$	$\mathcal{RI}_{\mathcal{B}}$	$\sigma_{\mathcal{RI}_{\mathcal{B}}}$	$\mathcal{RI}_{\Delta}$	$\sigma_{\mathcal{RI}_{\Delta}}$
$-\pi/2$	0.0043	0.0056	0.0037	0.0042	0.0029	0.0060	0.0014	0.0020
$-3\pi/8$	0.153	0.024	0.022	0.010	0.020	0.015	0.133	0.020
$-\pi/4$	0.542	0.059	0.044	0.039	0.288	0.059	0.253	0.029
$-\pi/8$	0.884	0.082	0.054	0.063	0.735	0.094	0.149	0.021
0	0.98	0.11	0.085	0.077	0.97	0.11	0.0058	0.0048
$\pi/8$	0.898	0.086	0.054	0.067	0.783	0.097	0.115	0.018
$\pi/4$	0.509	0.045	0.019	0.041	0.278	0.046	0.231	0.013
$3\pi/8$	0.159	0.041	0.022	0.035	0.049	0.039	0.111	0.018
$\pi/2$	0.017	0.011	0.0078	0.0075	0.010	0.011	0.0066	0.0048

$$\sigma_{\mathcal{P},\text{stat}} = \sqrt{\sum_{\substack{\zeta=X,Y\\K=A,B}} \left[\sum_{i=1}^{N} \left(\frac{\partial \mathcal{P}}{\partial \zeta_{K,i}}\right)^2 \sigma^2_{\zeta_K}\right] + \sum_{\substack{\zeta=X,Y\\K=A,B\\K'\neq K=A,B}} \left[\sum_{j=1}^{N} \left(\frac{\partial \mathcal{P}}{\partial \zeta_{K,j}}\right)\left(\frac{\partial \mathcal{P}}{\partial \zeta_{K',j}}\right) \sigma_{\zeta_K \zeta_{K'}}\right]}, \tag{D14}$$

where N is the total number of detected photons. Note that for $\mathcal{P} = \Delta$, only terms with $K = A$ contribute to the uncertainty.

Furthermore, in order to quantify separately the uncertainty contribution associated with the local and nonlocal parts of the $\mathcal{RI}$ quantity in Eq. (7), we rewrite it as

$$\mathcal{RI} = \left|\frac{\mathcal{B}}{2\sqrt{2}}\right|^2 + \Delta^2 \equiv \mathcal{RI}_{\mathcal{B}} + \mathcal{RI}_{\Delta}, \tag{D15}$$

with $\mathcal{RI}_{\mathcal{B}} = |\mathcal{B}/2\sqrt{2}|^2$ and $\mathcal{RI}_{\Delta} = \Delta^2$ accounting, respectively, for the contributions of the nonlocal and local correlations to $\mathcal{RI}$. By exploiting Eqs. (D12)–(D14) with $\mathcal{P} = \mathcal{RI}_{\mathcal{B}}, \mathcal{RI}_{\Delta}$, we obtain the overall uncertainties $\sigma_{\mathcal{RI}_{\mathcal{B}}}$ and $\sigma_{\mathcal{RI}_{\Delta}}$ associated with $\mathcal{RI}_{\mathcal{B}}$ and $\mathcal{RI}_{\Delta}$, achieving a good estimate of the $\sigma_{\mathcal{RI}}$ amount due to nonlocal and local correlations (although the intertwining between local and nonlocal terms in $\sigma_{\mathcal{RI}}$ makes it impossible to write it as $\sigma_{\mathcal{RI}} = \sqrt{\sigma^2_{\mathcal{RI}_{\mathcal{B}}} + \sigma^2_{\mathcal{RI}_{\Delta}}}$).

A detailed uncertainty budget is reported in Tables II–IV.

[1] M. Lucamarini, Z. L. Yuan, J. F. Dynes, and A. J. Shields, Overcoming the rate-distance limit of quantum key distribution without quantum repeaters, Nature **557**, 400 (2018).

[2] F. Xu, X. Ma, Q. Zhang, H.-K. Lo, and J.-W. Pan, Secure quantum key distribution with realistic devices, Rev. Mod. Phys. **92**, 025002 (2020).

[3] S. Pirandola, *et al.*, Advances in quantum cryptography, Adv. Opt. Photon. **12**, 1012 (2020).

[4] D. Dequal, L. T. Vidarte, V. R. Rodriguez, G. Vallone, P. Villoresi, A. Leverrier, and E. Diamanti, Feasibility of satellite-to-ground continuous-variable quantum key distribution, npj Quantum Inf. **7**, 3 (2021).

[5] Y.-A. Chen, *et al.*, An integrated space-to-ground quantum communication network over 4,600 kilometres, Nature **589**, 214 (2021).

[6] C. Clivati, *et al.*, Coherent phase transfer for real-world twin-field quantum key distribution, Nat. Commun. **13**, 157 (2022).

[7] H.-S. Zhong, *et al.*, Quantum computational advantage using photons, Science **370**, 1460 (2020).

[8] L. S. Madsen, *et al.*, Quantum computational advantage with a programmable photonic processor, Nature **606**, 75 (2022).

[9] A. J. Daley, I. Bloch, C. Kokail, S. Flannigan, N. Pearson, M. Troyer, and P. Zoller, Practical quantum advantage in quantum simulation, Nature **607**, 667 (2022).

[10] I. Cong, H. Levine, A. Keesling, D. Bluvstein, S.-T. Wang, and M. D. Lukin, Hardware-efficient, fault-tolerant quantum computation with Rydberg atoms, Phys. Rev. X **12**, 021049 (2022).

[11] Y. Kim, *et al.*, Evidence for the utility of quantum computing before fault tolerance, Nature **618**, 500 (2023).

[12] G. Brida, M. Genovese, and I. Ruo Berchera, Experimental realization of sub-shot-noise quantum imaging, Nat. Photonics **4**, 227 (2010).

[13] G. Brida, M. Genovese, A. Meda, and I. Ruo Berchera, Experimental quantum imaging exploiting multimode spatial correlation of twin beams, Phys. Rev. A **83**, 033811 (2011).

[14] M. Genovese, Real applications of quantum imaging, J. Opt. **18**, 073002 (2016).

[15] A. Meda, E. Losero, N. Samantaray, F. Scafirimuto, S. Pradyumna, A. Avella, I. Ruo Berchera, and M. Genovese, Photon-number correlation for quantum enhanced imaging and sensing, J. Opt. **19**, 094002 (2017).

[16] P.-A. Moreau, E. Toninelli, T. Gregory, and M. J. Padget, Imaging with quantum states of light, Nat. Rev. Phys. **1**, 367 (2019).

[17] C. A. Casacio, L. S. Madsen, A. Terrasson, M. Waleed, K. Barnscheidt, B. Hage, M. A. Taylor, and W. P. Bowen, Quantum-enhanced nonlinear microscopy, Nature **594**, 201 (2021).

[18] G. Ortolano, E. Losero, S. Pirandola, M. Genovese, and I. Ruo-Berchera, Experimental quantum reading with photon counting, Sci. Adv. **7**, abc7796 (2021).

[19] E. Martínez Vargas, C. Hirche, G. Sentís, M. Skotiniotis, M. Carrizo, R. Muñoz-Tapia, and J. Calsamiglia, Quantum sequential hypothesis testing, Phys. Rev. Lett. **126**, 180502 (2021).

[20] G. Ortolano, P. Boucher, I. P. Degiovanni, E. Losero, M. Genovese, and I. Ruo-Berchera, Quantum conformance test, Sci. Adv. **7**, abm3093 (2021).

[21] A. Karsa, A. Fletcher, G. Spedalieri, and S. Pirandola, Quantum illumination and quantum radar: A brief overview, Rep. Prog. Phys. **87**, 094001 (2024).

[22] V. Giovannetti, S. Lloyd, and L. Maccone, Advances in quantum metrology, Nat. Photonics **5**, 222 (2011).

[23] L. Pezzè, A. Smerzi, M. K. Oberthaler, R. Schmied, and P. Treutlein, Quantum metrology with nonclassical states of atomic ensembles, Rev. Mod. Phys. **90**, 035005 (2018).

[24] M. Barbieri, Optical quantum metrology, PRX Quantum **3**, 010202 (2022).

[25] A. Fallani, M. A. C. Rossi, D. Tamascelli, and M. G. Genoni, Learning feedback control strategies for quantum metrology, PRX Quantum **3**, 020310 (2022).

[26] P. Yin, *et al.*, Experimental super-Heisenberg quantum metrology with indefinite gate order, Nat. Phys. **19**, 1122 (2023).

[27] I. Aharonovich and E. Neu, Diamond nanophotonics, Adv. Opt. Mat. **2**, 911 (2014).

[28] E. Bernardi, R. Nelz, S. Sonusen, and E. Neu, Nanoscale sensing using point defects in single-crystal diamond: Recent progress on nitrogen vacancy center-based sensors, Crystals **7**, 124 (2017).

[29] C. L. Degen, F. Reinhard, and P. Cappellaro, Quantum sensing, Rev. Mod. Phys. **89**, 035002 (2017).

[30] S. Pirandola, B. R. Bardhan, T. Gehring, C. Wedbrook, and S. Lloyd, Advances in photonic quantum sensing, Nat. Photonics **12**, 724 (2018).

[31] S. Olivares, High-precision innovative sensing with continuous-variable optical states, Riv. Nuovo Cim. **41**, 341 (2018).

[32] G. Petrini, G. Tomagra, E. Bernardi, E. Moreva, P. Traina, A. Marcantoni, F. Picollo, K. Kvaková, P. Cígler, I. P. Degiovanni, V. Carabelli, and M. Genovese, Nanodiamond–quantum sensors reveal temperature variation associated to hippocampal neurons firing, Adv. Sci. **9**, 2202014 (2022).

[33] S. Virzì, A. Avella, F. Piacentini, M. Gramegna, T. Opatrný, A. G. Kofman, G. Kurizki, S. Gherardini, F. Caruso, I. P. Degiovanni, and M. Genovese, Quantum Zeno and anti-Zeno probes of noise correlations in photon polarization, Phys. Rev. Lett. **129**, 030401 (2022), and references therein.

[34] S. Virzì, *et al.*, Sensing microscopic noise events by frequent quantum measurements, Phys. Rev. Appl. **21**, 034014 (2024).

[35] N. Brunner, D. Cavalcanti, S. Pironio, V. Scarani, and S. Wehner, Bell nonlocality, Rev. Mod. Phys. **86**, 419 (2013 (2024).

[36] A. Einstein, B. Podolsky, and N. Rosen, Can quantum-mechanical description of physical reality be considered complete?, Phys. Rev. **47**, 777 (1935).

[37] J. S. Bell, On the Einstein Podolsky Rosen paradox, Physics **1**, 195 (1964).

[38] M. Genovese., Research on hidden variable theories: A review of recent progresses, Phys. Rep. **413**, 319 (2005).

[39] B. S. Tsirelson, Quantum generalizations of Bell's inequality, Lett. Math. Phys. **4**, 93 (1980).

[40] N. Linden, S. Popescu, A. J. Short, and A. Winter, Quantum nonlocality and beyond: Limits from nonlocal computation, Phys. Rev. Lett. **99**, 180502 (2007).

[41] M. Pawlowski, T. Paterek, D. Kaszlikowski, V. Scarani, A. Winter, and M. Zukowski, Information causality as a physical principle, Nature **461**, 1101 (2009).

[42] J. Oppenheim and S. Wehner, The uncertainty principle determines the non-locality of quantum mechanics, Science **330**, 1072 (2010).

[43] M. Navascués and H. Wunderlich, A glance beyond the quantum model, Proc. R. Soc. Lond. A **466**, 881 (2010).

[44] W. van Dam, Implausible consequences of superstrong nonlocality, Nat. Comput. **12**, 9 (2013).

[45] T. Fritz, A. B. Sainz, R. Augusiak, J. Bohr Brask, R. Chaves, A. Leverrier, and A. Acín, Local orthogonality as a multipartite principle for quantum correlations, Nat. Commun. **4**, 2263 (2013).

[46] H. F. Hofmann, Local measurement uncertainties impose a limit on nonlocal quantum correlations, Phys. Rev. A **100**, 012123 (2019).

[47] S. Popescu and D. Rohrlich, Quantum nonlocality as an axiom, Found. Phys. **24**, 379 (1994).

[48] A. Carmi and E. Cohen, Relativistic independence bounds nonlocality, Sci. Adv. **5**, eaav8370 (2019).

[49] E. Cohen and A. Carmi, In praise of quantum uncertainty, Entropy **22**, 302 (2020).

[50] A. Carmi and E. Cohen, On the significance of the quantum mechanical covariance matrix, Entropy **20**, 500 (2018).

[51] Y. Aharonov, D. Z. Albert, and L. Vaidman, How the result of a measurement of a component of the spin of a spin-1/2 particle can turn out to be 100, Phys. Rev. Lett. **60**, 1351 (1988).

[52] N. W. M. Ritchie, J. G. Story, and R. G. Hulet, Realization of a measurement of a weak value, Phys. Rev. Lett. **66**, 1107 (1991).

[53] J. Dressel, M. Malik, F. M. Miatto, A. N. Jordan, and R. W. Boyd, Colloquium: Understanding quantum weak

values: Basics and applications, Rev. Mod. Phys. **86**, 307 (2014).
[54] J. S. Lundeen and A. M. Steinberg, Experimental joint weak measurement on a photon pair as a probe of Hardy's paradox, Phys. Rev. Lett. **102**, 020404 (2009).
[55] M. Ringbauer, D. N. Biggerstaff, M. A. Broome, A. Fedrizzi, C. Branciard, and A. G. White, Experimental joint quantum measurements with minimum uncertainty, Phys. Rev. Lett. **112**, 020401 (2014).
[56] O. Calderón-Losada, T. T. Moctezuma Quistian, H. Cruz-Ramirez, S. M. Ramirez, A. B. U'Ren, A. Botero, and A. Valencia, A weak values approach for testing simultaneous Einstein-Podolsky-Rosen elements of reality for non-commuting observables, Commun. Phys. **3**, 117 (2020).
[57] A. C. Martinez-Becerril, G. Bussieres, D. Curic, L. Giner, R. A. Abrahao, and J. S. Lundeen, Theory and experiment for resource-efficient joint weak-measurement, Quantum **5**, 599 (2021).
[58] G. Mitchison, R. Jozsa, and S. Popescu, Sequential weak measurement, Phys. Rev. A **76**, 062105 (2007).
[59] G. S. Thekkadath, L. Giner, Y. Chalich, M. J. Horton, J. Banker, and J. S. Lundeen, Direct measurement of the density matrix of a quantum system, Phys. Rev. Lett. **117**, 120401 (2016).
[60] F. Piacentini, *et al.*, Measuring incompatible observables by exploiting sequential weak values, Phys. Rev. Lett. **117**, 120402 (2016).
[61] A. Avella, F. Piacentini, M. Borsarelli, M. Barbieri, M. Gramegna, R. Lussana, F. Villa, A. Tosi, I. P. Degiovanni, and M. Genovese, Anomalous weak values and the violation of a multiple-measurement Leggett-Garg inequality, Phys. Rev. A **96**, 052123 (2017).
[62] F. Piacentini, A. Avella, M. Gramegna, R. Lussana, F. Villa, A. Tosi, G. Brida I.P. Degiovanni, and M. Genovese, Investigating the effects of the interaction intensity in a weak measurement, Sci. Rep. **8**, 6959 (2018).
[63] Y. Kim, Y. S. Kim, S. Y. Lee, S. Moon, Y. H. Kim, and Y. W. Cho, Direct quantum process tomography via measuring sequential weak values of incompatible observables, Nat. Commun. **9**, 192 (2018).
[64] G. Foletto, M. Padovan, M. Avesani, H. Tebyanian, P. Villoresi, and G. Vallone, Experimental test of sequential weak measurements for certified quantum randomness extraction, Phys. Rev. A **103**, 062206 (2021).
[65] M. Bell and S. Gao, (eds.) *Quantum Nonlocality and Reality: 50 Years of Bell's Theorem* (Cambridge University Press, Cambridge, United Kingdom, 2016).
[66] R. Bertlmann and A. Zeilinger, (eds.) *Quantum [Un]Speakables II: Half a Century of Bell's Theorem* (Cham, Springer International Publishing, 2017).
[67] W. Myrvold, M. Genovese, and A. Shimony, Bell's Theorem. *The Stanford Encyclopedia of Philosophy*, edited by Edward N. Zalta (Metaphysics Research Laboratory, Stanford University), Fall 2021.
[68] J. Uffink, Quadratic Bell inequalities as tests for multipartite entanglement, Phys. Rev. Lett. **88**, 230406 (2002).
[69] B. S. Tsirelson, Quantum analogues of the Bell inequalities. The case of two spatially separated domains, J. Sov. Math. **36**, 557 (1987).
[70] L. J. Landau, Empirical two-point correlation functions, Found. Phys. **18**, 449 (1988).
[71] L. Masanes, Necessary and sufficient condition for quantum-generated correlations, arXiv:quant-ph/0309137.
[72] A. Cabello, Proposed experiment to test the bounds of quantum correlations, Phys. Rev. Lett. **92**, 060403 (2004).
[73] S. Filipp and K. Svozil, Generalizing Tsirelson's bound on Bell inequalities using a min-max principle, Phys. Rev. Lett. **93**, 130407 (2004).
[74] S. Wehner, Tsirelson bounds for generalized Clauser-Horne-Shimony-Holt inequalities, Phys. Rev. A **73**, 022110 (2006).
[75] M. Navascués, S. Pironio, and A. Acín, Bounding the set of quantum correlations, Phys. Rev. Lett. **98**, 010401 (2007).
[76] K. T. Goh, J. Kaniewski, E. Wolfe, T. Vértesi, X. Wu, Y. Cai, Y.-C. Liang, and V. Scarani, Geometry of the set of quantum correlations, Phys. Rev. A **97**, 022104 (2018).
[77] B. G. Christensen, Y. C. Liang, N. Brunner, N. Gisin, and P. G. Kwiat, Exploring the limits of quantum nonlocality with entangled photons, Phys. Rev. X **5**, 041052 (2015).
[78] J. A. Gubner, *Probability and Random Processes for Electrical and Computer Engineers* (Cambridge University Press, Cambridge, United Kingdom, 2006).
[79] L. Maccone, Dagmar Bruß, and C. Macchiavello, Complementarity and correlations, Phys. Rev. Lett. **114**, 130401 (2015).
[80] A. Kumari, A. K. Pan, and P. K. Panigrahi, Joint weak value for all order coupling using continuous variable and qubit probe, Eur. Phys. J. D **71**, 275 (2017).
[81] M. Genovese, Interpretations of quantum mechanics and measurement problem, Adv. Sci. Lett. **3**, 249 (2010).
[82] A. Shimony, in *Proceedings of the International Symposium Foundations of Quantum Mechanics in the Light of New Technology* (Central Research Laboratory, Tokyo, Japan, August 29–31, 1983), p. 225.
[83] A. Shimony, in *Quantum Concepts in Space and Time*, edited by R. Penrose and C. J. Isham (Oxford University Press, New York, 1986), p. 182.
[84] M. Barbieri, F. De Martini, G. Di Nepi, and P. Mataloni, Towards a test of non-locality without "supplementary assumptions", Phys. Lett. A **334**, 23 (2005).
[85] N. Gisin, Quantum nonlocality: How does nature do it? Science **326**, 1357 (2009).
[86] D. Cavalcanti, M. L. Almeida, V. Scarani, and A. Acín, Quantum networks reveal quantum nonlocality, Nat. Commun. **2**, 184 (2011).
[87] L. Aolita, R. Gallego, A. Acín, A. Chiuri, G. Vallone, P. Mataloni, and A. Cabello, Fully nonlocal quantum correlations, Phys. Rev. A **85**, 032107 (2012).
[88] M. Ringbauer, C. Giarmatzi, R. Chaves, F. Costa, A. G. White, and A. Fedrizzi, Experimental test of nonlocal causality, Sci. Adv. **2**, e1600162 (2016).
[89] N. Gisin, J. Bancal, Y. Cai, P. Remy, A. Tavakoli, E. Zambrini Cruzeiro, S. Popescu, and N. Brunner, Constraints on nonlocality in networks from no-signaling and independence, Nat. Commun. **11**, 2378 (2020).
[90] L. Wooltorton, P. Brown, and R. Colbeck, Tight analytic bound on the trade-off between device-independent randomness and nonlocality, Phys. Rev. Lett. **129**, 150403 (2022).

[91] C. Marletto and V. Vedral, Interference in quantum field theory: Detecting ghosts with phases, Ann. Phys. **535**, 2200530 (2023).

[92] N. N. Wang, A. Pozas-Kerstjens, C. Zhang, B. H. Liu, Y. F. Huang, C. F. Li, G. C. Guo, N. Gisin, and A. Tavakoli, Certification of non-classicality in all links of a photonic star network without assuming quantum mechanics, Nat. Commun. **14**, 2153 (2023).

[93] A. Cabello, Minimum full nonlocality, all versus nothing nonlocality, and quantum pseudo telepathy, arXiv:2311.17735.

[94] M. Pettini, Quantum entanglement: Proposal for a new kind of experiment, arXiv:2311.17070.

[95] M. Genovese and M. Gramegna, Quantum correlations and quantum non-locality: A review and a few new ideas, Appl. Sci. **9**, 5406 (2019).

[96] R. Jozsa and N. Linden, On the role of entanglement in quantum-computational speed-up, Proc. R. Soc. Lond. A **459**, 2011 (2003).

[97] D. Gross, S. T. Flammia, and J. Eisert, Most quantum states are too entangled to be useful as computational resources, Phys. Rev. Lett. **102**, 190501 (2009).

[98] L. Lami, C. Hirche, G. Adesso, and A. Winter, Schur complement inequalities for covariance matrices and monogamy of quantum correlations, Phys. Rev. Lett. **117**, 220502 (2016).

[99] F. Madonini, F. Severini, A. Incoronato, E. Conca, and F. Villa, in *Proc. of SPIE 11771, Quantum Optics and Photon Counting 2021* (2021), p. 117710B.

[100] Yu.I. Bogdanov, G. Brida, M. Genovese, S. P. Kulik, E. V. Moreva, and A. P. Shurupov, Statistical estimation of the efficiency of quantum state tomography protocols, Phys. Rev. Lett. **105**, 010404 (2010).

[101] E. Rebufello, *et al.*, Protective measurement—a new quantum measurement paradigm: Detailed description of the first realization, Appl. Sci. **11**, 4260 (2021).

[102] E. Rebufello, *et al.*, Anomalous weak values via a single photon detection, Light: Sci. & Appl. **10**, 106 (2021).

[103] A. G. Kofman, S. Ashhab, and F. Nori, Nonperturbative theory of weak pre-and post-selected measurements, Phys. Rep. **520**, 43 (2012).

[104] B. Tamir and E. Cohen, Introduction to weak measurements and weak values, Quanta **3**, 7 (2013).